

See discussions, stats, and author profiles for this publication at: <https://www.researchgate.net/publication/266624950>

Polyion Complex Micelle Based on Albumin–Polymer Conjugates: Multifunctional Oligonucleotide Transfection Vectors for Anticancer Chemotherapeutics

ARTICLE *in* BIOMACROMOLECULES · OCTOBER 2014

Impact Factor: 5.75 · DOI: 10.1021/bm501205x · Source: PubMed

CITATIONS

4

READS

171

5 AUTHORS, INCLUDING:



[Yanyan Jiang](#)

University of New South Wales

22 PUBLICATIONS 120 CITATIONS

[SEE PROFILE](#)



[Hongxu Lu](#)

University of New South Wales

50 PUBLICATIONS 733 CITATIONS

[SEE PROFILE](#)



[Aydan Dağ](#)

Bezmiâlem Vakıf Üniversitesi

33 PUBLICATIONS 841 CITATIONS

[SEE PROFILE](#)



[Martina H Stenzel](#)

University of New South Wales

279 PUBLICATIONS 11,052 CITATIONS

[SEE PROFILE](#)

Polyion Complex Micelle Based on Albumin–Polymer Conjugates: Multifunctional Oligonucleotide Transfection Vectors for Anticancer Chemotherapeutics

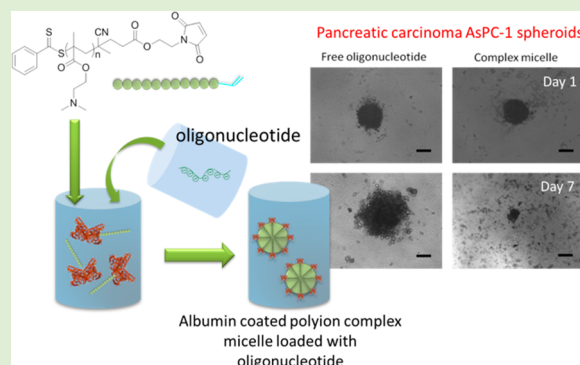
Yanyan Jiang,[†] Hongxu Lu,[†] Yee Yee Khine,[†] Aydan Dag,^{†,‡} and Martina H. Stenzel*,[†]

[†]Centre for Advanced Macromolecular Design (CAMD), School of Chemistry, University of New South Wales, Sydney, NSW 2052, Australia

[‡]Department of Pharmaceutical Chemistry, Faculty of Pharmacy, Bezmialem Vakif University, 34093 Fatih, Istanbul, Turkey

S Supporting Information

ABSTRACT: Novel biocompatible polyion complex micelles, containing bovine serum albumin (BSA), polymer, and oligonucleotide, were synthesized as a generation of vectors for the gene transfection. Maleimide-terminated poly((N,N-dimethyl amino) ethyl methacrylate) (PDMAEMA) was prepared via reversible addition–fragmentation chain transfer (RAFT) polymerization and subsequently deprotected. Precise one to one albumin–PDMAEMA bioconjugates have been achieved via 1,4-addition with the free thiol group on Cys34 on the BSA protein. SDS-PAGE and GPC (water) confirmed and quantified the successful conjugation. The conjugation efficiency was found to be independent of the molecular weight of PDMAEMA. After careful pH adjustment, the conjugate could efficiently condense anticancer oligonucleotide, ISIS 5132, which resulted in particles of 15–35 nm with a negative zeta-potential. The size was easily controlled by the polymer chain length. The albumin corona provides complete protection of the cationic polymer and genetic drug, which gave rise to lower potential toxicity from the polymer and higher gene transfection efficiency. Although a control experiment with a traditional PEG-based polyion complex micelle could deliver the drug just as effectively, if not more so, to the ovarian cancer cell line OVCAR-3, this carrier had no selectivity toward cancerous cells and proved just as toxic to HS27 (fibroblast) cell line. In contrast, the albumin-coated particles demonstrated desirable selectivity toward cancerous cells and have been shown to have outstanding performance in the cytotoxicity tests of several carcinoma monolayer cell models. In addition, the complex micelles were able to destroy pancreatic multicellular tumor spheroids, while free ISIS 5132 could not penetrate the spheroid at all. Hence, albumin-coated/oligonucleotide complex micelles are far more promising than the most classical gene delivery vectors.



INTRODUCTION

Safe and efficient transfection of nucleic acid-based drugs (like oligonucleotide and short interfering RNA (siRNA)) to desired site, with the assistance of vectors, has been of considerable interest in the nanomedicine field in the past few decades.^{1–3}

Within this field, effective gene transfection holds great importance for the treatment of a wide variety of diseases, and a successful transfection vehicle, once developed, might have a wider range of applications.⁴ Specifically, antisense oligonucleotides (ASOs), which are short single strands of DNA, have been utilized successfully as therapeutic agents since they can potentially inhibit the expression or activity of mutated or foreign genes as well as permanently replace a missing or deficient gene.⁵ Gene transfection is a highly promising technique to improve the efficiency and use of ASOs as a potential therapeutic agent for the treatment of genetic diseases, like carcinomas.⁶ To date, several critical barriers still restrict their application in a clinical setting. In addition to low stability against degradation by the serum nucleases, which

limits their use,⁷ ASOs also possess a relatively high molecular weight, which may hamper cellular uptake. Their residence time in the plasma is therefore insufficient to allow them to reach their site of action in the body at the therapeutic concentrations required.⁸

Despite tremendous academic efforts and ongoing clinical trials on oligonucleotide transfection, none of the existing vectors are generally acceptable for human gene therapy. Initially, conventional biological carriers like viruses were investigated to promote transfection efficiency.⁹ In terms of gene therapy vectors, the viral particles encapsulate a therapeutic gene cassette in place of the viral genome and introduce functional genetic information expressed from the recombinant vectors into the targeting cells.⁹ However, some of the drawbacks of biological carriers include variations during

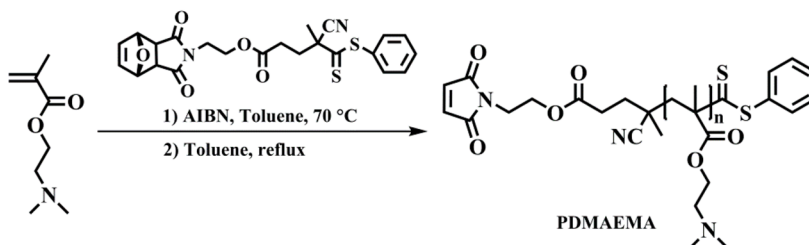
Received: August 16, 2014

Revised: October 1, 2014

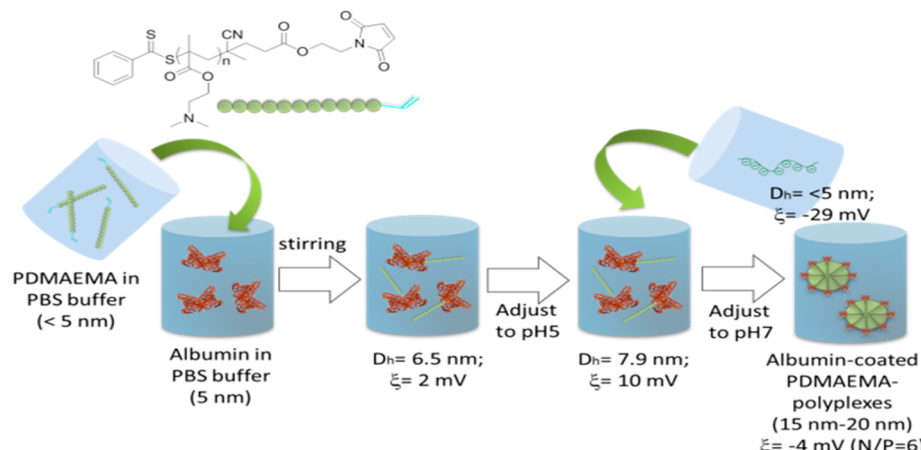
Published: October 7, 2014

Scheme 1. RAFT Polymerization of DMAEMA, End-Group Deprotection via Retro-Diels-Alder Reaction, Conjugation of PDMAEMA and Albumin, and Formation of Complex Micelles

Synthesis of PDMAEMA with maleimide end group



Polyion complex micelles



fabrication, low transfection efficiency and immunogenicity.^{10,11} These limitations incentivized research into synthetic vectors as an alternative transfection agent. Polymeric gene delivery systems, typically cationically charged polymers, such as polyethylenimine (PEI), poly-L-lysine, and poly(2-dimethylaminoethyl methacrylate) (PDMAEMA),^{12,13} have been intensively investigated as a means to condense oligonucleotides into nanoparticles. The advantages over viral carriers include minimal host immune response, high stability in storage and ease of production in large quantities.¹⁴ Nevertheless, it cannot be neglected that the use of cationic polymers is partly hampered because of their cytotoxicity,¹⁵ and compared to biological carriers, polymeric vectors often lack cell selectivity.

Effective methods for delivering genetic materials into cells must not only meet all the demands outlined above, but the approach must also be simple and commercially viable before the clinical potential of gene therapy can be fully realized.¹⁶ An ideal gene transfection vector should combine the merits of viral and nonviral vectors. Among the available potential colloidal drug carrier systems, protein-based nanocarriers are particularly intriguing.¹⁷ Many formulations for hydrophobic drugs use albumin as a carrier with the drug either physically encapsulated, chemically bound to single albumin molecules, or processed into albumin particles.¹⁸ According to pathophysiological properties of the cancerous cells, high amounts of albumin accumulate in tumors where metabolism in the carcinoma site is enhanced by specific receptor glycoprotein gp60 on the endothelial cell surface. The receptor provides a transport pathway for albumin carriers to the subendothelial space and more importantly, gives rise to a targeted distribution

of the drug in tumor tissues.^{18,19} However, the direct use of BSA to deliver genetic drugs cannot be directly employed due to the negative charge of albumin which would repel the negatively charged nucleic acids. In some cases, albumin has been modified to allow for conjugation to genetic drugs.^{20,21} Albumin was modified either by reacting the carboxylic groups on albumin with amines^{22,23} or by coating the albumin with cationic polymers such as polyethylenimine (PEI),²⁴ which then condensed DNA. In most cases, the size of the carriers were well above 200 nm, albeit fine-tuning of the reaction conditions could generate highly efficient carrier for transfection agents.²⁵ However, extensive modification of albumin will affect the structure of the protein and, thus, properties unique to albumin such as their increased transendothelial gp60 (the 60-kDa glycoprotein)-mediated transport and increased intratumoral accumulation as a result of the SPARC (Secreted Protein, Acidic and Rich in Cysteine)—albumin interaction.²⁶ A pathway to modify albumin without affecting its bioactivity is to modify only one amino acid, Cys 34, with a water-soluble cationic polymer as has been widely applied using other polymeric systems.^{27–29} This method results in a unique structure which not only retains the functions of native albumin but also has the capability to condense genetic drugs to form the nanoparticles. As for the cationic polymer candidates, poly((*N,N*-dimethylamino) ethyl methacrylate) (PDMEA), which has repeatedly been used to condense oligonucleotides and DNA,^{8,30} is a promising choice for attachment to albumin due to its buffering capacity, lower cytotoxicity, and ease of preparation via controlled living polymerization.³¹

The aim of this work is to develop a multifunctional vector for oligonucleotide transfection, which meets the demands of high safety, biocompatibility, efficiency, and selectivity. In this research, we developed a method of polyion complex micelle formation through a combination of conventional gene condensation and one-pot protein polymer conjugation to generate an albumin-based drug carrier to transfect the oligonucleotide ISIS 5132, which has a high anticancer activity.³² The technology incorporates three vital steps: the precise polymerization and deprotection of end-functionalized PDMAEMA, the conjugation of albumin to polymer, and the condensation of oligonucleotide via electrostatic interaction (Scheme 1). The condensation of the oligonucleotide took place simultaneously with the formation of polyion complex micelles. These biohybrid micelles possess a built-in biofunctionality through the presence of the albumin based headgroup when compared to a PEG-based hydrophilic headgroup, as typically used for polymeric micelles.⁷ The polyion complex micelles were tested in their ability to deliver ISIS 5132 using the established 2D cancerous cell model followed by a 3D pancreatic multicellular tumor spheroid model. BSA was chosen as the reactive albumin due to the easy access and this early stage of the investigation. SPARC synthesized by bovine, porcine, and human cells demonstrated a high affinity binding to BSA³³ and it is probably a reasonably good model. However, the use of HAS may be considered.

EXPERIMENTAL SECTION

Chemicals. Unless otherwise stated, all chemicals were reagent grade and used as received. 4',4-Azobis(4-cyanopentanoic acid) (Fluka, 98%), 4-(dimethylamino)pyridine (DMAP, Aldrich, >99%), acetonitrile (Aldrich, 99.8%), anhydrous methanol (Sigma-Aldrich, 99.8%), benzyl chloride (Aldrich, 99%), bovine serum albumin (BSA, Sigma, >96%), chloroform-D (CIL, 99.8%), dimethylacetamide (DMAc, Sigma-Aldrich, 99.9%), elemental sulfur (Ajax, 98%), ethyl acetate (Ajax, 99%), furan (Aldrich, >99%), hydrochloric acid (Ajax, 31.5% w/w), maleic anhydride (Fluka, >99%), n-hexane (Ajax, >95%), N,N'-dicyclohexylcarbodiimide (DCC, Aldrich, 99%), poly(ethylene glycol) methyl ether methacrylate (PEGMEMA, $M_n = 300 \text{ g}\cdot\text{mol}^{-1}$, Aldrich, reagent), silica gel (Sigma-Aldrich, 60 Å, 70–230 mesh), sodium methoxide (Fluka, >97%), sodium phosphate dibasic (Sigma-Aldrich, 98%), sodium phosphate monobasic (Sigma-Aldrich, >99%), sodium hydroxide (Aldrich, 98%), sodium chloride (Univar, reagent), ethylenediaminetetraacetic acid (EDTA, Sigma-Aldrich, reagent), DNA quantitation kit (Sigma, 1 mg/mL), and toluene (Ajax, 99%) were used as received. The oligonucleotides (ISIS5132, sequence (5'-3'): TCCCCGCCT-GTGACATGCATT; molecular weight, 6044 g·mol⁻¹) were purchased from Sigma. 2,2-Azobis(isobutyronitrile) (AIBN, Fluka, 98%) was purified by recrystallization from methanol. The synthesis of 4-cyanopentanoic acid dithiobenzoate (CPADB) and the subsequent furan protected maleimide-terminated product (MCPADB) are described elsewhere (Scheme S1).¹⁹ N,N-Dimethylamino ethyl methacrylate (DMAEMA, Aldrich, 98%) was purified by passing through a column of activated basic alumina to remove the inhibitor.

Syntheses. Synthesis of PDMAEMA via RAFT Polymerization. DMAEMA (14.15 g, 0.09 mol), RAFT agent MCPADB (0.36 g, 7.5×10^{-4} mol), and initiator AIBN (0.025 g, 1.5×10^{-4} mol) were dissolved in toluene to achieve a ratio of [monomer]/[RAFT]/[initiator] = 120:1:0.1 to achieve a concentration of 1.5 mol/mL relative to the monomer. The reaction mixture was divided equally into three vials sealed and purged with nitrogen for 1 h at 0 °C. The polymerization was carried out in an oil bath at 70 °C where the vials were reacted for 3, 5, and 7 h, respectively. The reaction was terminated by placing the vials in an ice bath for 5 min and introducing air. The same procedure was also used to prepare higher molecular weight PDMAEMA where the initial ratio of [monomer]/[RAFT]/

[initiator] = 350:1:0.1. Finally, the polymer was precipitated in cyclohexane and dried under reduced pressure. The conversion and the theoretical molecular weight (M_n) was determined by ¹H NMR (CDCl_3). The polydispersity index (D) was measured by gel permeation chromatography (GPC) using DMAc as the mobile phase.

Deprotection of the Furan Protected Maleimide End Group on PDMAEMA. A total of 1.3 g polymer was dissolved in 50 mL of toluene and the solution was refluxed at 110 °C for 7 h to remove the furan protecting group. The solvent was evaporated and the product was further dried with under vacuum to give the targeted maleimide terminated PDMAEMA. The formation of maleimide group was confirmed by ¹H NMR with the presence of new proton peak at 6.75 ppm.

Conjugation of Albumin and PDMAEMA. A stock solution of both PDMAEMA ($M_n = 21700 \text{ g}\cdot\text{mol}^{-1}$) and BSA were prepared where each compound was dissolved in PBS (pH 7.4, with 20 mM EDTA) buffer at a concentration of 1 mM. The two solutions were then mixed at different ratios at the ambient temperature. The molar ratios of BSA and PDMAEMA were 1:1, 5:1, 10:1, and 20:1, respectively. Each mixture was stirred for 18 h to facilitate the thiol–ene click reaction between the thiol group on the BSA and the maleimide group at the end of the PDMAEMA polymer chain. The product was purified via dialysis in PBS buffer (pH 5) and the solvent was changed every 2 h for 12 h. The dialysis of the sample aimed to remove the residual amount of EDTA and adjust the pH of the final solution to 5. The conjugates of albumin and PDMAEMA with different chain length with a ratio of 2:1 were obtained using the same procedure.

Formation of Polyion Complex Micelles from Albumin–PDMAEMA Conjugates and ISIS 5132. Solutions of albumin–PDMAEMA conjugates with required albumin to PDMAEMA ratios were prepared. The resulting conjugates were dialyzed in 0.05 M PBS (pH 5) for 12 h by changing solvent every 2 h. Solutions of ISIS 5132 in Milli-Q water at different concentrations were added dropwise to the conjugate solutions (pH 5) to yield a polyion complex micelle with certain nitrogen/phosphorus (N/P) ratios. The complex was immediately used after ISIS 5132 addition since the complex had a tendency to agglomerate. Alternatively, adjusting the pH value to pH 7 resulted in the formation of a micelle solution which was stable over an extended period of time. Given that cells grow in a neutral environment, the latter procedure was preferred. In addition, a control experiment was carried out using bovine genome DNA fragments (Sigma-Aldrich) instead of ISIS 5132. All the conditions of synthesis remained consistent with the procedure described for preparing ISIS 5132 oligonucleotide complex micelles. In addition, we also investigated the oligonucleotide transfection efficiency of the PEGMEMA-PDMAEMA cationic block copolymer. The same protocol was adopted to make the polyion complex micelles from this polymer solution. The route of the polymerization of this copolymer is provided in the Supporting Information.

The effect of pH value on the structure of BSA was investigated by analyzing the fluorescence emission profiles of the tryptophan residues. Stock solutions of BSA (pH 7), BSA (pH 5), and polymer–BSA conjugate (1 mg mL⁻¹) were prepared and diluted. Fluorescence measurements were then carried at an excitation wavelength of 300 nm and with the emission spectra was recorded in the wavelength region of 250–550 nm.

Cell Culture. Human ovarian carcinoma (OVCAR-3) cells, human pancreatic carcinoma (AsPC-1) cells, human prostate carcinoma (LNCaP) cells, and fibroblast (HS27) cells were cultured in tissue culture flasks with RPMI 1640 medium (supplemented with 10% fetal bovine serum, sodium pyruvate, penicillin and streptomycin) at 37 °C under a 5% CO₂ atmosphere. After reaching confluence, cells were collected from the flasks with trypsin/EDTA treatment. The cell suspension was used for the further experiments.

Analysis. Proton Nuclear Magnetic Resonance (¹H NMR) Spectroscopy. All NMR measurements were performed using a Bruker DPX-300 with a ¹H/X inverse broadband z gradient BBI probe at 300 MHz frequency and 16 scans as default. Samples were dissolved and analyzed in deuterated chloroform (CDCl_3).

Dynamic Light Scattering (DLS). The particle size, size distribution, and zeta potential of polyion micelles were measured using DLS. The concentration of albumin is 1 mg mL⁻¹, and the concentration of the oligonucleotide is 0.2 mg/mL. The data were obtained using Malvern Nano-ZS as particle size analyzer (laser, 4 mW, $\lambda = 632$ nm; measurement angle 12.8° and 175°). Measurements were run for at least three times at 25 °C.

Fluorescence Spectroscopy. Fluorescence spectroscopy was carried out at 25 °C with Cary Eclipse fluorescence spectrophotometer. Both of the excitation and emission slits were set at 5 nm. The measurements were conducted in a four-sided glass cuvette at 200 nm/second scan rate.

DMAc Gel Permeation Chromatography (DMAc GPC). DMAc GPC measurements were performed using a Shimadzu modular system containing a DGU-12A degasser, an LC-10AT pump, a SIL-10AD automatic injector, a CTO-10A column oven and a RID-10A refractive index detector. A 50 × 7.8 mm guard column and four 300 × 7.8 mm columns (500, 10³, 10⁴, and 10⁵ Å pore size, 5 μm particle size) were used for analyses. DMAc (HPLC grade, 0.05% w/v BHT, 0.03% w/v LiBr) with a flow rate of 1 mL·min⁻¹ was used as the mobile phase. The injection volume was 50 μL. The samples were prepared by dissolving the samples in DMAc at a concentration of 2–3 mg·mL⁻¹, followed by filtration through a 0.45 μm filter. The unit was calibrated using commercially available linear polystyrene standards (0.5–1000 kDa, Polymer Laboratories). Chromatograms were processed using Cirrus 2.0 software (Polymer Laboratories).

Water Gel Permeation Chromatography (Water GPC). Water GPC (Milli-Q water containing 0.02% w/v NaN₃) was performed using a Shimadzu modular system comprising a DGU-12A solvent degasser, an LC-10AT pump, a CTO-10A column oven, and a RID-10A refractive index detector (flow rate: 0.8 mL·min⁻¹). The system was equipped with a Polymer Laboratories 5.0 mm bead-size guard column (50 × 7.8 mm²) followed by three 300 × 7.8 mm PL columns (30, 40, and 50, respectively, in type). Calibration was conducted with PEO standards ranging from 500 to 500000 g·mol⁻¹.

Transmission Electron Microscopy (TEM). TEM analyses were performed using a FEI Tecnai-G2 at 80–100 kV beam voltage. Samples were prepared by placing a drop of solution on carbon-coated copper grids and draining the excess with filter paper. Samples were stained with uranyl acetate (2% aqueous solution) and then air-dried for 2 min.

Ethidium Bromide Displacement Assay. The ethidium bromide displacement assay was employed according to the methods described elsewhere.³⁴ Excitation wavelength ($\lambda = 480$ nm) and emission wavelength ($\lambda = 605$ nm) of ethidium bromide (EtBr) were obtained using a Cary Eclipse fluorescence spectrophotometer (Agilent Technologies) with a slit width of 5 nm. The fluorescence intensity of EtBr (10 μg·mL⁻¹) was initially measured as background before ISIS 5132 oligonucleotide solutions, at different concentrations, were added to 100 μL of EtBr solution. The mixtures were brought to the same volume and the fluorescence intensity was measured to determine the saturation point of EtBr to oligonucleotide. The saturated oligonucleotide/EtBr complex was also titrated with the five cationic albumin–polymer conjugates and tracked by fluorescence spectrophotometer.

Cellular Uptake Observed Using Laser Scanning Confocal Microscopy. OVCAR-3 cells were seeded in 35 mm Fluorodish (World Precision Instruments) at a density of 60000 cells per dish and cultured for 3 days with RPMI 1640 medium supplemented with 10% fetal bovine serum. Micelle solutions were loaded to OVCAR-3 cells at a working concentration of 50 μg·mL⁻¹ and incubated at 37 °C for 2 h. After incubation, the cells were washed thrice with PBS (pH 7.4). The cells were then stained with Hoechst 33342 for 10 min followed by staining with 100 nM Lysotracker Red DND-99 (Invitrogen) for 1 min. The dye solution was quickly removed and the cells were gently washed with PBS. Finally, the cells were mounted in PBS and observed under a laser scanning confocal microscope system (Zeiss LSM 780). The system was equipped with a Diode 405–30 laser, an argon laser and a DPSS 561–10 laser (excitation and absorbance wavelengths: 405, 488, and 561 nm, respectively) connected to a Zeiss Axio

Observer. The ZEN2011 imaging software (Zeiss) was used for image acquisition and processing.

Cytotoxicity Testing. The cell suspensions of OVCAR-3 (ovarian cancer), HS27 (fibroblast), AsPC-1 (pancreatic cancer), and LNCaP (prostate cancer) cell lines were seeded into 96-well cell culture plates at a cell density of 40000 cells·mL⁻¹, 100 μL·well⁻¹, and incubated for 1 day at 37 °C and 5% CO₂. The medium in the cell culture plate was then discarded and replaced with 100 μL of fresh twice-concentrated RPMI1640 medium and the cells were incubated with the micelle solutions for 48 h. Before loading into the cell culture plates, the micelle solutions were prepared by sterilization by UV irradiation for 20 min, and then serial dilution (in Milli-Q water) where each micelle solution was half the concentration of the solution before it. The cell viability was then determined with sulforhodamine B (SRB) assay. The culture medium was discarded and 100 μL of 10% TCA was added to each well, followed by incubation of the plates for 30 min at 4 °C. The supernatant was discarded and the plates washed 5 times with DI water. A total of 100 μL of SRB solution 0.4% (w/v) in 1% acetic acid was added to each well, and the plates were incubated for 15 min at room temperature. After staining, any unbound dye was removed by washing five times with 1% acetic acid and the plates were air-dried. Bound stains were solubilized with 200 μL of 10 mM Tris buffer and absorbance was measured on a Bio-Rad BenchMark microplate reader ($\lambda = 490$ nm), with data analyzed and plotted using GraphPad Prism 6.0.

Pancreatic Multicellular Tumor Spheroid (MCTS) Preparation and Drug Treatment. The cell density of AsPC-1 suspension was adjusted to 1.0×10^5 cells·mL⁻¹. A total of 10 μL of cell suspension was gently dropped onto the lid of a 100 mm cell culture dish. The lid was then slowly turned over and placed onto the dish filled with 10 mL sterile PBS to maintain the humidity of inner dish chamber. The cells were incubated and kept undisturbed at 37 °C at 5% CO₂. After culture for 7 days, the MCTS were transferred to a 96-well suspension culture plate (Corning) and cultured for 1 day before further experiments. Sterile Milli-Q water (as a control), oligonucleotide, and oligonucleotide complex micelles were added to the spheroids which have been cultured for 1 day in the 96-well suspension culture plates. The morphology of the MCTS at day 0 and after 7 days was recorded using a Leica DM IL inverted microscope equipped with a ProgRes Scan camera (Warner Instruments, LLC), and the sizes were analyzed using the software ProgRes CapturePro.

RESULTS AND DISCUSSION

The initial step is the formation of bioconjugates between albumin and PDMAEMA, and the researcher can choose from an array of techniques.^{35,36} Herein, a protected maleimide chain transfer agent was chosen for the polymerization of DMAEMA, which was followed by deprotection to give the expected α -functional polymer (Scheme 1).³⁷ A series of protected PDMAEMA polymers with different molecular weights were synthesized using the RAFT process. The conversion for each sample was determined by ¹H NMR (CDCl₃) and the molecular weight and the polydispersity (D) were evaluated by DMAc GPC, and the results are listed in Table 1. From ¹H NMR characterization, the group fidelity was found to be well above 95%.

Subsequently, a retro Diels–Alder reaction was used as the deprotection procedure and was carried out by refluxing the protected polymers in toluene under nitrogen atmosphere (Scheme 1). The success of the retro-Diels–Alder reaction was confirmed using ¹H NMR where the signals at 6.5, 5.3, and 2.8 ppm disappeared and were replaced by a signal at 6.75 ppm belonging to the newly formed double bond (SI, Figure S1). The reactive polymer then undergoes conjugation to albumin via the only available thiol functional group on Cys 34 to create a protein with a single polymer chain.³⁸ Although polymers can be conjugated to various functional groups on the protein,

Table 1. RAFT Polymerization of PDMAEMA

	[M]/[RAFT]/[I]	time (h)	con. ^a (%)	M_n^b (g mol ⁻¹)	GPC; ^c D	M_n^d (g mol ⁻¹)
1	120:1:0.1	3	42.6	8550	1.14	8450
2	120:1:0.1	5	55.7	10500	1.17	10450
3	120:1:0.1	7	74.5	14550	1.16	14450
4	350:1:0.1	5	38.7	21800	1.15	21700
5	350:1:0.1	16	84.4	47000	1.17	46900

^aObtained from ¹H NMR analysis. ^bCalculated from NMR. ^cDetermined from DMAc GPC (relative to PS standards). ^dAfter deprotection.

conjugation to this thiol with one polymer chain is the least likely to distort the protein structure.

Although the conjugation between polymers and BSA is a well-known procedure,^{39–41} to the best of our knowledge the specific conjugation of PDMAEMA to Cys 34 of albumin has not yet been described, although the conjugation to other proteins has been reported.⁴² Another example of PDMAEMA–BSA conjugates include the use of albumin to initialize the growth of multiple PDMAEMA chains, but this approach was found to affect the specific activity of BSA due to the large number of arms.⁴³ To investigate the conjugation efficiency with albumin, PDMAEMA with a $M_n = 21700$ g mol⁻¹ was employed as the amount of Cys34 available for reaction depends on the source of albumin. Conveniently, the amount of available Cys34 can be measured using Ellman's reagent⁴³ and it was determined that the albumin used in this work contained 60% active Cys34. The albumin was reacted with PDMAEMA at various ratios (Table 2) and the crucial aspect of this step was careful adjustment of the pH. At pH 7 the protein was negatively charged, while PDMAEMA was positively charged, which would only lead to electrostatic interaction between the two. Lowering the pH value to the isoelectric point (IEP) of albumin can at least neutralize the charges on the protein (Scheme 1). As shown in Table 2, the molar ratios of BSA and PDMAEMA in each sample were 1:1 (sample 5), 1:0.5 (sample 6), 1:0.1 (sample 7), and 1:0.05 (sample 8), respectively. After a reaction time of 18 h, the

success of the conjugation was determined using SDS-PAGE (Figure S2) and water GPC (Figure S3). The conjugation of BSA and PDMAEMA was verified with SDS-PAGE by the presence of bands at molecular weight at around 85 kDa, which is within the expected range (66 kDa for BSA and 21.7 kDa for PDMAEMA). The band at around 85 kDa loses its intensity simply because of the decreasing PDMAEMA content in the sample. GPC analysis in water was then employed to quantify the conjugation efficiency, calculated by the difference between initial BSA amount and the nonreacted BSA amount. According to the area of the water GPC peaks, the conjugation efficiency of BSA for the four samples is 39, 15, 7, and 6%, respectively, which correlates to 39, 70, 86, and >99% of reacted PDMAEMA. An excess of albumin is therefore required to achieve full functionalization, caused by the partial inactivity of albumin. At pH 5, DLS analysis (Table 2) revealed a hydrodynamic diameter of the protein conjugates (samples 5–8) similar to that of naked BSA (samples 2 and 3), indicating the presence of unimers. As expected, the zetapotential (ζ) of samples with increasing PDMAEMA content switched from a negative to a positive value as the structure became more similar to that of pure PDMAEMA (sample 4, $\zeta = 7.63$ mV). At this point in time it is possible to purify the product by HPLC analysis. The product was however used without further purification since albumin is present in abundance in cell growth media and in the blood.

Polyion complex micelles, prepared from cationic block copolymers and anionic drugs such as nucleic acids, are widely employed for the safe delivery of these drugs.⁴⁴ Herein, we use albumin, the main constituent in blood plasma, to replace PEG which is commonly used for polymeric drug delivery. Albumin, is not only potentially biocompatible and biodegradable, it also enhances the delivery to the tumor site due to its high affinity to the tumor tissue.⁴⁵ Albumin–polymer conjugates/oligonucleotide polyion complexes were obtained via the electrostatic interactions between the cationic polymer and the negatively charged oligonucleotide. The subsequent condensation of the oligonucleotide to form polyion complex micelles required careful quenching of the charges on albumin (IEP at pH 4.7,

Table 2. Hydrodynamic Diameter and Zeta Potential of the Relevant Materials and the Complexes^a

sample number	molar ratio			N/P ratio	pH	D_h (nm)	zeta potential ζ (mV)	IC ₅₀ (μ g/mL)
	BSA	PDMAEMA	oligonucleotide					
1			1		7	0–107	-29.87	>>604
2	1				7	5.4	-5.64	
3	1				5	6.28	-2.53	
4		1			7	N/A	7.63	
5	1	1			5	6.16	2.04	
6	1	0.2			5	5.17	0.51	
7	1	0.1			5	5.43	-0.82	
8	1	0.05			5	6.01	-2.15	
9	1	1	0.6	ISIS5132	12	7	-4.16	4.94
10	1	0.2	0.6		2.4	7	-9.07	17.13
11	1	0.1	0.6		1.2	7	-10.8	>>100
12	1	0.05	0.6		0.6	7	-12.4	>>100
13	1	1	NA	inactive DNA	12	7	-5.23	126.4
14	1	0.2	NA		2.4	7	-10.7	128
15	1	0.1	NA		1.2	7	-9.7	>>100
16	1	0.05	NA		0.6	7	-12.1	>>100
17	1	0.5	0.4	ISIS5132	4	7	-7.11	8.55

^aConcentration of albumin in relevant samples is 1 mg/mL, and concentration of oligonucleotide is 0.2 mg/mL.

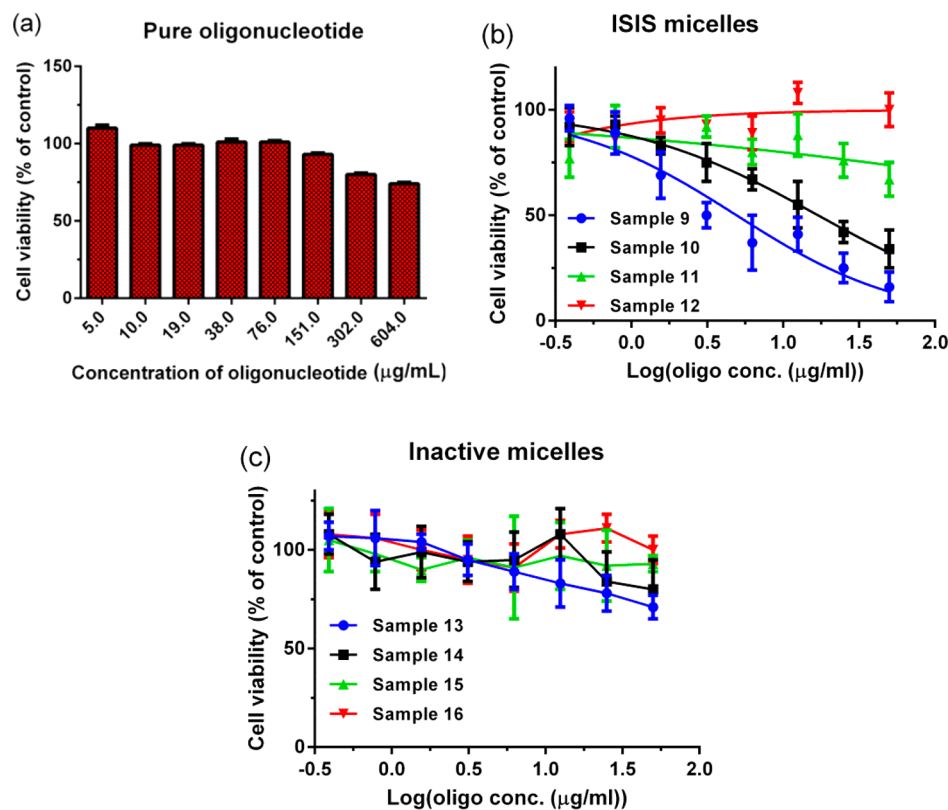


Figure 1. Cytotoxicity assays of free oligonucleotide, albumin–polymer conjugates/DNA complex micelle, and albumin–polymer conjugates/oligonucleotide complex micelle against OVCAR-3 ovarian cancer cells for 48 h. (a) Cytotoxicity test of pure oligonucleotide against OVCAR-3 cells for 48 h. (b) Cytotoxicity test of oligonucleotide (ISIS 5132) complex against OVCAR-3 cells for 48 h. From sample 9–12, the N/P ratio is 12, 2.4, 1.2 and 0.6, respectively. (c) Cytotoxicity test of inactive DNA fragment against OVCAR-3 cells for 48 h. From sample 13–16, the N/P ratio is 12, 2.4, 1.2 and 0.6, respectively. Values represent the mean \pm SD.

which renders the protein negatively charged at pH 7) to ensure that the electrostatic interaction will take place predominately between oligonucleotide and PDMAEMA and not the protein. The condensation of the oligonucleotide was therefore carried out at pH 5 and the ISIS 5132 oligonucleotide, dissolved in Milli-Q water at a concentration of $200 \mu\text{g}\cdot\text{mL}^{-1}$ ($\zeta = -29.87 \text{ mV}$), was added slowly. As listed in Table 2, when sample 5 was added to the ISIS 5132 solution (N/P ratio = 12), the resulting polyion complex micelles have sizes of 12–15 nm ($\zeta = -0.41 \text{ mV}$ at pH 5 and $\zeta = -4.16 \text{ mV}$ at pH 7). The complex of sample 6 and the oligonucleotide (sample 10) was also found to be stable. However, small amounts of PDMAEMA and a large excess of BSA led to aggregation, most likely caused by albumin’s natural tendency to aggregate. For oligonucleotide complexes, which were stable at pH 5, the pH of the solution was increased to 7 to protect the complexes. The increase in pH increased the surface charge of particles, thereby stabilizing the complexes against aggregation. It is interesting to note that the resulting particles have a negative surface charge, which is partly caused by the presence of the negatively charged oligonucleotide, but it also indicates that the cationic polymer is located within the core of the micelle.

Since BSA was held at pH 5 for 30 min, the stability of BSA needs to be investigated. BSA is stable at pH 7 but rapidly degrades via aggregation and hydrolysis at pH 2.⁴⁶ Fluorescence analysis of the tryptophan residue can be directly correlated to the degradation of the protein.⁴⁷ BSA was directly compared to the albumin–polymer conjugate at pH 5. The sample chosen

has been stored at 4 °C for three months to evaluate in addition the long-term stability. The emission maxima were in all cases located at 349 nm (SI, Figure S3). The apparent decline in intensity is due to the lower concentration of the albumin–polymer conjugate in the solution. Overall, it seems that the preparation had only a small effect on the stability of BSA.

Prior to any further investigations in regards to the binding efficiency between the protein conjugate and ISIS 5132 and further optimization, the albumin–polymer conjugates (samples 5–8; Table 2) were used to evaluate the toxicity of the drug carrier itself, but also to investigate the question if the drug, ISIS 5132, is still active when trapped inside the polyion complex micelle. To investigate the toxicity of the drug carrier, the albumin–polymer conjugates (samples 5–8) were condensed with inactive bovine genome DNA fragments (nontoxic) instead of ISIS 5132. The albumin–polymer conjugates were incubated with bovine genome DNA at the same concentrations to generate the inactive micelles of similar sizes (samples 13–16, Table 2). As shown in Table 2, the concentrations of albumin and oligonucleotide (or bovine genome DNA fragments) were kept constant in all experiments, and only the amount of the polymer attached was varied. Although the ISIS 5132 does not show any toxicity toward OVCAR-3 cells at the measured concentrations, the toxicity increases quickly with increasing amounts of albumin–polymer conjugates indicating the safe delivery of the oligonucleotide into the cell (Figure 1a and Figure 1b). The carrier, loaded with DNA only, showed only negligible cytotoxicity (Figure 1c). The dominant fraction of cell death

can therefore be assigned to the effective transfection of ISIS 5132. The complex micelle with the highest amount of PDMAEMA (sample 9) showed the highest toxicity indicating the safe delivery of the drug and its release. With a high N/P ratio of 12 in sample 9, the oligonucleotide was safely condensed into small particles with only a slight negative surface charge. This resulted in efficient cellular uptake nanoparticles, while the drug could obviously escape the complex micelle once inside the cell. However, one downside is that a higher PDMAEMA fraction led to a slightly higher toxicity.

Based on the aforementioned results, the ratio of BSA to PDMAEMA was set to be 2 to 1 as an effective and biologically safe conjugation ratio. The influence of the polymer chain length on the performance was focus of the following investigation. Five polymers with different chain length (Table 1) were employed to achieve the bioconjugation with albumin (named as C8K, C10k, C14K, C21K, and C47K, respectively, where the number represents the molecular weight of the polymer in g/mol). Figure 2 depicts the SDS-PAGE of

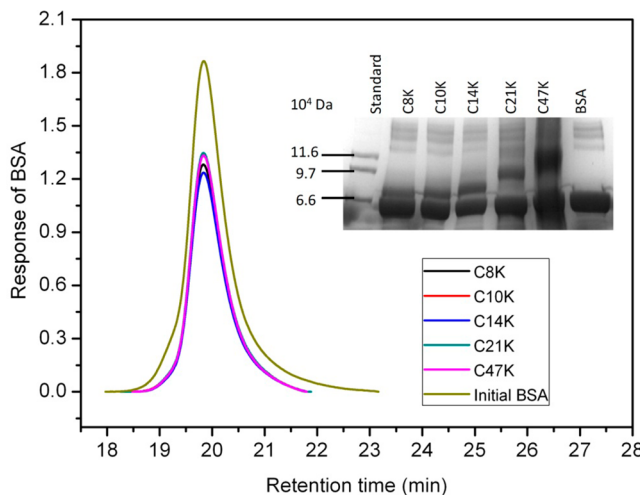


Figure 2. Water GPC traces of the initial BSA (olive) and the BSA residuals after reaction. The inset is the corresponding SDS-PAGE shift for the conjugation of BSA and PDMAEMA with different chain length.

the conjugation between albumin and PDMAEMA. The band relating to the conjugate clearly shifts to higher molecular weight with increasing polymer size. The water GPC curves further indicated that the polymer chain length has no effect on thiol–ene reaction activity and the amount of reacted albumin was found to be approximately 40% across all five samples. This equated to 80% of the available PDMAEMA undergoing a reaction with BSA.

Studies to assess the binding efficiency of all the aforementioned polymer–protein conjugates were carried out using the ethidium bromide (EtBr) displacement assay. If EtBr is added to oligonucleotide, a strong fluorescence is seen because of the highly fluorescent complex between oligonucleotide and EtBr. However, if the addition of another compound causes the decreasing of fluorescence intensity, then it means that the EtBr has been displaced, demonstrating stronger bonding between the oligonucleotide and the sample. Herein, the oligonucleotide/EtBr (saturated according to Figure S4) complex was titrated with the five cationic albumin–polymer

conjugates, respectively, and the fluorescence intensity was monitored by the fluorescence spectrophotometer, as shown in Figure 3. The rapid decreasing of the fluorescence intensity

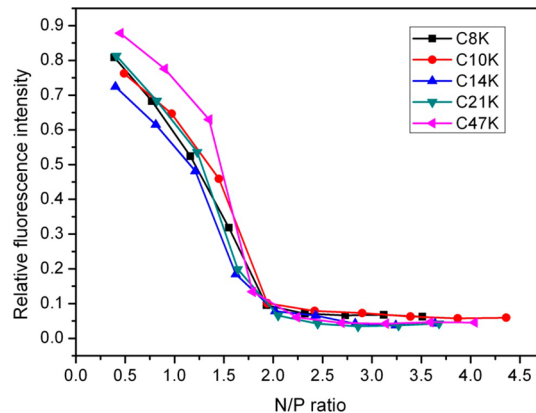


Figure 3. Ethidium bromide displacement by albumin–PDMAEMA conjugates and gene complexes in PBS (pH 7).

demonstrates the binding between the polymer–protein conjugates and oligonucleotides has a saturation point at an N/P ratio of around 2.5, which is independent of the molecular weight of PDMAEMA.

The complex formation was studied in more depth using agarose gel shift assays. In this assay, results were obtained by monitoring the position of the bands of uncomplexed oligonucleotide which were stained by EtBr. The oligonucleotide was only visible if it was accessible by EtBr to form a complex which generates strong fluorescence. Three different batches of complex micelle samples were investigated: in experiment 1 (Figure 4a), samples were loaded to the gel immediately after the binding of the conjugates and the oligonucleotide, while in experiment 2 (Figure 4b), samples were incubated for 8 h to achieve maximum binding before loading to the agarose gel. In both cases, EtBr was added directly into the running buffer. In experiment 3 (Figure 4c), EtBr was first added to the free oligonucleotide to form the saturated complex (according to Figure S4), followed by the addition of the polymer–protein conjugates to force the replacement of EtBr. In each sample, the molar ratio of albumin, polymer, and oligonucleotide was kept constant (2:1:1), which leads to different N/P ratios due to the different polymer chain length. The N/P ratios were calculated to be 2 (in C8K/oligo complex), 3 (in C10K/oligo complex), 4 (in C14K/oligo complex), 6 (in C21K/oligo complex), and 14 (in C46K/oligo complex), respectively. Upon inspection of Figure 4a,b, it becomes evident that most of the oligonucleotide was bound by the polymer–protein conjugates, and the benefits of longer incubation time is clearly distinct with all oligonucleotide being bound across all molecular weights. The type of binding can be identified when taking the results depicted in Figure 4c into account. The bands of free oligonucleotide in experiment 3 had fully disappeared. This results indicate that EtBr has been replaced by the cationic polymer because of the stronger electrostatic interaction between PDMAEMA and oligonucleotide. As a result, the complex micelle was formed with all available oligonucleotide tightly bound. Moreover, the binding of EtBr to oligonucleotide leads to strong fluorescent bands in the neutral position. Compared to Figure 4a,c, the brightness of the bands in the

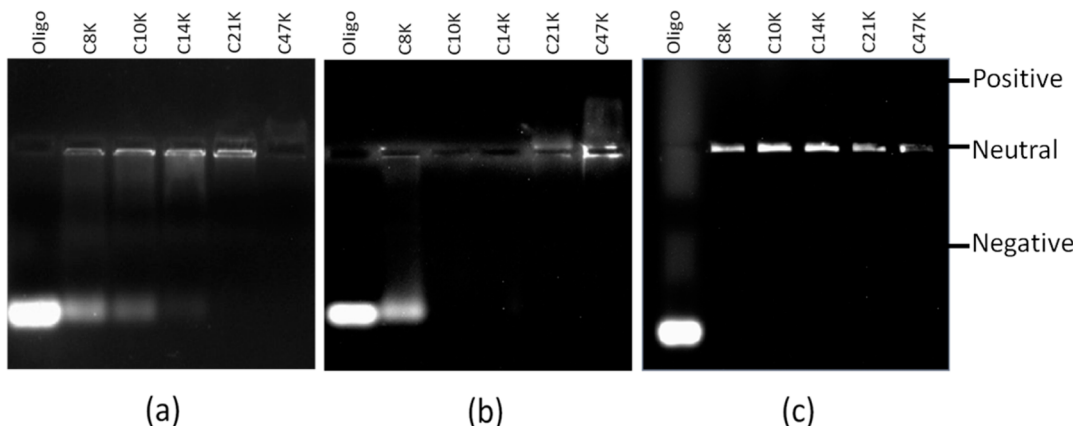


Figure 4. Agarose gel shift assays of the conjugates/oligo complex. (a) The shift of the complex after 15 min (EtBr loaded in running buffer); (b) the shift of the complex after 8 h (EtBr loaded in running buffer); (c) the shift of the complex after 8 h (ethidium bromide complex with oligonucleotide first). In the agarose gel image, oligonucleotide stands for the initial oligonucleotide and C8K stands for the free oligonucleotide after binding with the C8K conjugates and so on. N/P ratio: C8K/oligo = 2, C10K/oligo = 3, C14K/oligo = 4, C21K/oligo = 6, C47K/oligo = 14.

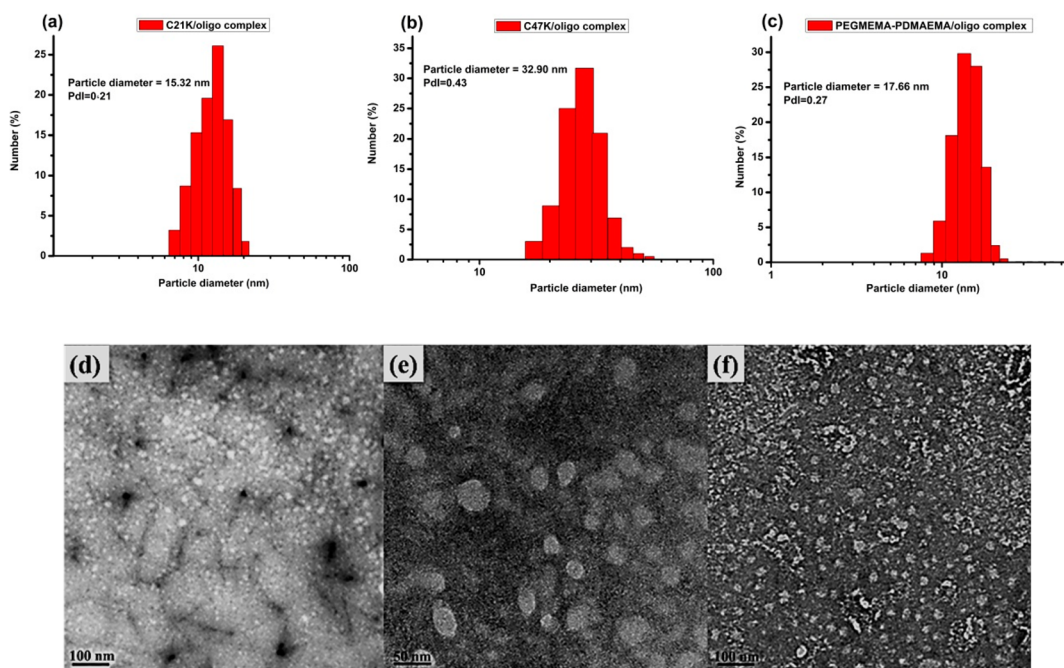


Figure 5. Size, distribution, and shape of (a, d) C21K/oligonucleotide; (b, e) C47K/oligonucleotide; (c, f) PEGMEMA-*b*-PDMAEMA/oligonucleotide polyion complex micelles, all at N/P = 4. (a–c) DLS measurements of the complex micelles and (d–f) the corresponding TEM images. The concentration of albumin is 1 mg/mL.

neutral position in Figure 4b is clearly reduced. In this scenario, the complex was allowed to optimize binding for 8 h causing the nanoparticle to compact. As a result, the EtBr in the running buffer could not penetrate into the micelles to stain the free oligonucleotide trapped inside the complex micelle. A comparison of Figure 4a and b reveals that it is necessary to incubate the complex for an extended period of time to optimize binding although it is not clear at this point in time if the full 8 h are necessary to achieve this. The agarose gel shift assay, which was recorded straight after mixing (Figure 4a), shows free oligonucleotide and a brightly lit neutral line indicative of easy penetration of EtBr into the complex.

Therefore, from the results given, a N/P ratio of 2.5–4 and an 8 h incubation time was sufficient to efficiently bind the oligonucleotide to form the BSA coated polyion complex micelles. Herein, a N/P ratio = 4 was chosen to build the gene

transfection vector in the following experiment. Prior to any in vitro investigation, a conventional polyion complex micelle with a PEG-type shell prepared from poly(oligoethylene glycol methacrylate) (PEGMEMA)-block-PDMAEMA (PEGMEMA-PDMAEMA) with the same N/P ratio was used to elucidate the effect of the BSA shell. Since most reported drug carriers for the delivery of nucleotides are based on PEG, a control experiment was included that compares a neutral micelle surface with the albumin surface. DLS analysis was employed to determine the hydrodynamic diameter of the conventional and the two BSA polyion complex micelles (Figure 5a–c). The conventional polyion complex micelle was observed to be similar in size to the one prepared from the polymer–protein conjugate, which was based on a PDMAEMA polymer of 21 kDa. PDMAEMA with a larger molecular weight led to larger particles, which is in agreement with earlier reports that

describe a correlation between the molecular weight of the polymer attached to the protein and the size of the resulting micelle.¹⁹ TEM analysis (Figure 5d–f) confirmed the particle size albeit the size is beyond the resolution of the TEM instrument.

Prior to detailed cytotoxicity investigations, the uptake of fluorescence-labeled polyion complex micelles by the cancer cells was monitored (Figure 6). The cell nuclei were stained

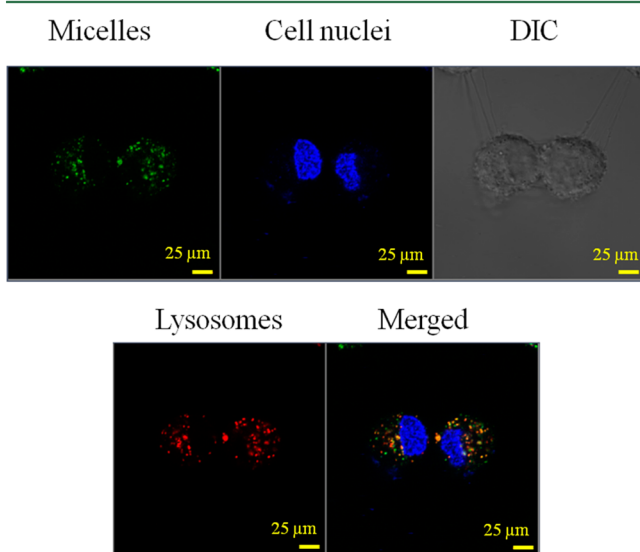


Figure 6. Confocal microphotographs of OVCAR-3 cells after incubation with C21K/DNA polyion complex micelles at 37 °C for 2 h. Albumin (green) was labeled with FITC. Cell nucleus (blue) was stained with Hoechst 33342, which also stained the encapsulated DNA. Lysosomes (Red) were stained with Lyso Tracker Red DND-99. Scale bar is 25 μ m.

blue with Hoechst 33342 and lysosomes were stained red with LysoTracker DND-99. The inactive DNA was used in this investigation to eliminate any toxic effects to the cell (which was partly stained blue). After incubation with the OVCAR-3 cells for 2 h, the micelles (BSA in green) were engulfed by the cells and could be located in the lysosomes (red). It was clearly evident that the oligonucleotide wrapped in the albumin complex micelles were safely transfected into the cells by endocytosis. The green and blue dot-like structures, which coincide with the location of the lysosomes, indicate the simultaneous uptake of the drug carrier and DNA.

It is hypothesized that the replacement of a typically used PEG corona of the polyion complex micelle by an albumin shell has an array of advantages in addition to the biocompatibility and the degradability. Therefore, a polyion complex micelle based on PEGMEMA-*b*-PDMAEMA and ISIS 5132 has been reported earlier as an efficient way to deliver the oligonucleotide.¹² Therefore, a similar block copolymer PEGMEMA₁₆₆-*b*-PDMAEMA₁₂₃ was synthesized using established procedures and tested alongside the albumin micelles to investigate the effect on the albumin shell to safely deliver the drug into cells. OVCAR-3 (ovarian cancer), AsPC-1 (pancreatic cancer), and LNCaP (prostate cancer) cell lines were employed to investigate the cell growth inhibition of these polyion complex micelles. In addition, HS27 as a noncancerous cell line was used as a control to evaluate the selectivity of the albumin–polymer conjugates/oligonucleotide complex micelles toward cancer cells. In vitro studies revealed that PEGMEMA₁₆₆-PDMAEMA₁₂₃/oligonucleotide complex micelles were toxic to the OVCAR-3 cell line, but the complex was even more toxic to the healthy HS27 cells (Figure 7). Compared to the free oligonucleotide, this enhanced efficiency is attributed to the change in uptake pathway where the drugs pass through the cell via endocytosis instead of diffusion. Nevertheless, the PEG-based micelles had no selectivity toward cancerous cells. This is

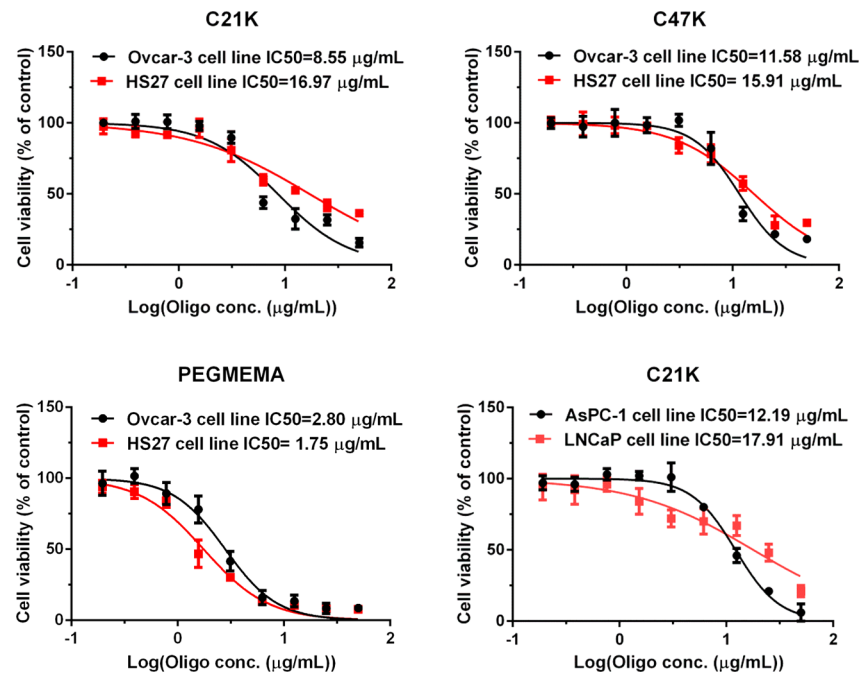


Figure 7. Cytotoxicity assays of C21K/Oligo complex micelle, C47K/Oligo complex micelle, and PEGMEMA₁₆₆-PDMAEMA₁₂₃/Oligo complex micelle against OVCAR-3 cancer cells and HS27 cells for 48 h. AsPC-1 and LNCaP cell lines were also tested. Values represent the mean \pm SD.

in contrast to the BSA-based micelle. The transfection efficiency of oligonucleotide delivered using albumin-coated micelles has also been improved compared to free ISIS 5132, albeit to a lesser extent than the PEG-based micelle. It is crucial to note, however, that the increased toxicity is more pronounced with cancerous cell than with healthy cells, indicating a higher selectivity toward cancerous cells. This can be attributed to the role of albumin in cell biology. Albumin binds to a receptor on the surface of the endothelial wall called gp60, which is also known as albomin. This receptor–ligand binding then causes the intracellular tail of the receptor to recruit caveolin-1, resulting in the formation of invaginations at the membrane surface that ultimately form transcytotic vesicles known as caveolae.⁴⁸ Gp60 cell expression has been found on cells other than the endothelial wall, such as HEPG2 cells (human hepatoliver carcinoma cells), which are overexpressed in order to internalize large amounts of albumin to fuel proliferation.⁴⁹ While no literature describe the presence of these receptors in ovarian cancer cell lines, its overexpression in cancerous cells such as HEPG2 imply that they may also be found on other cells as well, which then implies receptor-mediated endocytosis as a potential uptake pathway.²⁶ In conclusion, albumin introduces an element of selectivity toward cancer cell lines while the micelle based on PEGMEMA lead to an even higher toxicity in healthy cells compared to cancerous cells.

Strong support for the high efficacy of the albumin–polymer/oligonucleotide complex micelle was obtained when investigating the behavior in 3D AsPC-1 multicellular tumor spheroids. For *in vitro* cytotoxicity studies, compared to the monolayer cell testes, multicellular spheroids exhibit higher similarity to real tissues in terms of cell metabolism and gene profiles. They have recently attracted increasing research interests in non-medical fields.⁵⁰ The AsPC-1 spheroids were incubated with Milli-Q water (control), free oligonucleotide, or complex micelles for 7 d at 37 °C. The morphology of spheroids is shown in Figure 8 (more in Figures S4–6). The initial

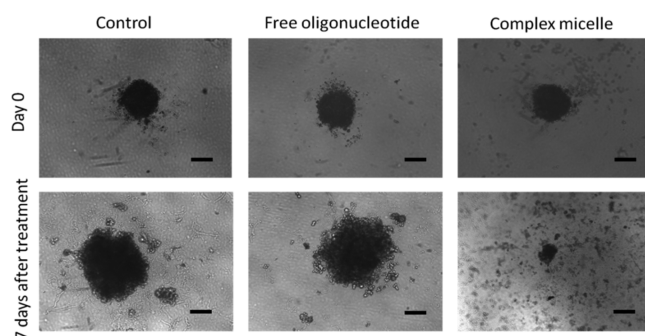


Figure 8. Pancreatic carcinoma AsPC-1 spheroids were treated with free oligonucleotide and C21K/Oligo complex micelle for 7 days. Scale bar = 200 μ m.

spheroids were approximately 350 μ m. After being treated for 7 days, the spheroid incubated in complex micelles showed an obvious inhibition to the cell proliferation. It could be observed that the whole spheroid structure has been destroyed with only a small core and cell residuals remaining, while the sizes of the AsPC-1 spheroids in the other two treatment groups increased to more than 500 μ m. As shown in Figure S7, the results were also in agreement with the DNA amount in each sample, which provides further evidence on the high gene transfection

efficiency of the albumin–polymer/oligonucleotide complex micelle.

CONCLUSIONS

In this work, we have demonstrated the successful fabrication of albumin–polymer conjugated nanocarriers and also its ability to transfet oligonucleotides into cancerous cells without losing the specificity of albumin. The conjugation efficiency of albumin and PDMAEMA, the appropriate ratio of albumin and PDMAEMA, the influence of the polymer chain length, and the complex efficiency of polyion complex micelles have been investigated in detail and they were found to be crucial to generate a drug-loaded carrier of high stability and high efficacy. Furthermore, this special albumin-based nanoparticle is able to selectively transfet the oligonucleotide to cancerous cells, while healthy cells are much less affected. In addition, the drug-loaded carrier was able to deplete pancreatic carcinoma AsPC-1 spheroids. In this work, we expanded the portfolio of albumin-based carriers to oligonucleotides while the design of the carrier still maintained the high selectivity of albumin.

ASSOCIATED CONTENT

Supporting Information

¹H NMR spectrum of PDMAEMA, SDS PAGE of the conjugation of BSA with PDMAEMA, GPC (water) curves of BSA before and after conjugation, fluorescence intensity of different EtBr and oligonucleotide ratios, fluorescence spectra of BSA and protein conjugates, and further images of spheroid cancers. This material is available free of charge via the Internet at <http://pubs.acs.org>.

AUTHOR INFORMATION

Notes

The authors declare no competing financial interest.

ACKNOWLEDGMENTS

The authors like to thank the Australian Research Council (ARC) for funding. A.D. acknowledges for the financial support from the The Scientific and Technological Research Council of Turkey (TUBITAK; Project No: 1059B191200208).

REFERENCES

- Zhou, Y.; Sharma, N.; Deshmukh, P.; Lakhman, R. K.; Jain, M.; Kasi, R. M. *J. Am. Chem. Soc.* **2012**, *134* (3), 1630–41.
- Jayakumar, R.; Chennazhi, K. P.; Muzzarelli, R. A. A.; Tamura, H.; Nair, S. V.; Selvamurugan, N. *Carb. Polym.* **2010**, *79* (1), 1–8.
- Deshpande, M. C.; Garnett, M. C.; Vamvakaki, M.; Bailey, L.; Armes, S. P.; Stolnik, S. J. *Controlled Release* **2002**, *81* (1–2), 185–199.
- Menon, J. U.; Ravikumar, P.; Pise, A.; Gyawali, D.; Hsia, C. C. W.; Nguyen, K. T. *Acta Biomater.* **2014**, *10* (6), 2643–2652.
- Ma, D. D. F.; Le Doan, T. *Ann. Int. Med.* **1994**, *120* (2), 161–163.
- Mullen, P.; McPhillips, F.; Monia, B. P.; Smyth, J. F.; Langdon, S. P. *Int. J. Cancer* **2006**, *118* (6), 1565–71.
- Chang, C.-W.; Bays, E.; Tao, L.; Alconcel, S. N. S.; Maynard, H. D. *Chem. Commun.* **2009**, *0* (24), 3580–3582.
- Seo, J. H.; Matsuno, R.; Lee, Y.; Takai, M.; Ishihara, K. *Biomaterials* **2009**, *30* (28), 4859–67.
- Kay, M. A.; Glorioso, J. C.; Naldini, L. *Nat. Med.* **2001**, *7* (1), 33–40.
- Rhaese, S.; von Briesen, H.; Rübsamen-Waigmann, H.; Kreuter, J.; Langer, K. *J. Controlled Release* **2003**, *92* (1–2), 199–208.
- Luo, D.; Saltzman, W. M. *Nat. Biotechnol.* **2000**, *18* (1), 33–7.

- (12) Zhang, L.; Nguyen, T. L. U.; Bernard, J.; Davis, T. P.; Barner-Kowollik, C.; Stenzel, M. H. *Biomacromolecules* **2007**, *8* (9), 2890–2901.
- (13) Chung, Y.-C.; Hsieh, W.-Y.; Young, T.-H. *Biomaterials* **2010**, *31* (14), 4194–4203.
- (14) Stenzel, M. H. *Chem. Commun.* **2008**, No. 30, 3486–503.
- (15) Lee, H.; Lytton-Jean, A. K. R.; Chen, Y.; Love, K. T.; Park, A. I.; Karagiannis, E. D.; Sehgal, A.; Querbes, W.; Zurenko, C. S.; Jayaraman, M.; Peng, C. G.; Charisse, K.; Borodovsky, A.; Manoharan, M.; Donahoe, J. S.; Truelove, J.; Nahrendorf, M.; Langer, R.; Anderson, D. G. *Nat. Nano* **2012**, *7* (6), 389–393.
- (16) Chen, J. P.; Yang, H. J.; Hoffman, A. S. *Biomaterials* **1990**, *11* (9), 625–30.
- (17) Garanger, E.; Lecommandou, S. *Angew. Chem.* **2012**, *S1* (13), 3060–3062.
- (18) Elsadek, B.; Kratz, F. *J. Controlled Release* **2012**, *157* (1), 4–28.
- (19) Jiang, Y.; Liang, R.; Svejkar, D.; Lu, H.; Hart-Smith, G.; Scarano, W.; Stenzel, M. H. *Chem. Commun.* **2014**, *50*, 6394–6397.
- (20) Chilkoti, A.; Chen, G.; Stayton, P. S.; Hoffman, A. S. *Bioconjugate Chem.* **1994**, *5* (6), 504–7.
- (21) Fischer, D.; Bieber, T.; Brüsselbach, S.; Elsässer, H.-P.; Kissel, T. *Int. J. Pharm.* **2001**, *225* (1–2), 97–111.
- (22) Dirks, A. T.; Cornelissen, J. J.; Nolte, R. J. *Bioconjugate Chem.* **2009**, *20* (6), 1129–38.
- (23) Shibata, H.; Nakagawa, S.; Tsutsumi, Y. *Molecules* **2005**, *10* (1), 162–80.
- (24) Kendrick, B. S.; Kerwin, B. A.; Chang, B. S.; Philo, J. S. *Anal. Biochem.* **2001**, *299* (2), 136–46.
- (25) Eisele, K.; Gropeanu, R. A.; Zehendner, C. M.; Rouhanipour, A.; Ramanathan, A.; Mihov, G.; Koynov, K.; Kuhlmann, C. R. W.; Vasudevan, S. G.; Luhmann, H. J.; Weil, T. *Biomaterials* **2010**, *31* (33), 8789–8801.
- (26) Elzoghby, A. O.; Samy, W. M.; Elgindy, N. A. *J. Controlled Release* **2012**, *157* (2), 168–182.
- (27) Heredia, K. L.; Maynard, H. D. *Org. Biomol. Chem.* **2007**, *5* (1), 45–53.
- (28) Dirks, A. J.; Nolte, R. J. M.; Cornelissen, J. J. L. M. *Adv. Mater.* **2008**, *20* (20), 3953–3957.
- (29) Le Droumaguet, B.; Velonia, K. *Angew. Chem.* **2008**, *120* (33), 6359–6362.
- (30) Hickey, R. J.; Haynes, A. S.; Kikkawa, J. M.; Park, S. J. *J. Am. Chem. Soc.* **2011**, *133* (5), 1517–25.
- (31) Agarwal, S.; Zhang, Y.; Maji, S.; Greiner, A. *Mater. Today* **2012**, *15* (9), 388–393.
- (32) Stevenson, J. P.; Yao, K.-S.; Gallagher, M.; Friedland, D.; Mitchell, E. P.; Cassella, A.; Monia, B.; Kwoh, T. J.; Yu, R.; Holmlund, J.; Dorr, F. A.; O'Dwyer, P. J. *J. Clin. Oncol.* **1999**, *17* (7), 2227.
- (33) Sage, H.; Johnson, C.; Bornstein, P. *J. Biol. Chem.* **1984**, *259* (6), 3993–4007.
- (34) Palacio, L.; Ho, C. C.; Prádanos, P.; Hernández, A.; Zydny, A. *L. J. Membr. Sci.* **2003**, *222* (1–2), 41–51.
- (35) Macewan, S. R.; Chilkoti, A. *Nano Lett.* **2012**, *12* (6), 3322–8.
- (36) Mantovani, G.; Lecolley, F.; Tao, L.; Haddleton, D. M.; Clerx, J.; Cornelissen, J. J. L. M.; Velonia, K. *J. Am. Chem. Soc.* **2005**, *127* (9), 2966–2973.
- (37) Suda, T.; Liu, D. *Mol. Ther.* **2007**, *15* (12), 2063–9.
- (38) Carter, D. C.; Ho, J. X., Structure of Serum Albumin. In *Advances in Protein Chemistry*; Anfinsen, J. T. E. F. M. R.; David, S. E., Eds.; Academic Press: New York, 1994; Vol. 45, pp 153–203.
- (39) Bays, E.; Tao, L.; Chang, C.-W.; Maynard, H. D. *Biomacromolecules* **2009**, *10* (7), 1777–1781.
- (40) Tao, L.; Xu, J. T.; Cell, D.; Davis, T. P. *Macromolecules* **2010**, *43* (8), 3721–3727.
- (41) Shakya, A. K.; Sami, H.; Srivastava, A.; Kumar, A. *Prog. Polym. Sci.* **2010**, *35* (4), 459–486.
- (42) van Dijk-Wolthuis, W. N. E.; van de Wetering, P.; Hinrichs, W. L. J.; Hofmeyer, L. J. F.; Liskamp, R. M. J.; Crommelin, D. J. A.; Hennink, W. E. *Bioconjugate Chem.* **1999**, *10* (4), 687–692.
- (43) Zhang, J.; Lei, Y.; Dhaliwal, A.; Ng, Q. K. T.; Du, J.; Yan, M.; Lu, Y.; Segura, T. *Biomacromolecules* **2011**, *12* (4), 1006–1014.
- (44) Zhao, Y.; Lord, M. S.; Stenzel, M. H. *J. Mater. Chem. B* **2013**, *1* (11), 1635–1643.
- (45) Elsadek, B.; Kratz, F. *J. Controlled Release* **2012**, *157* (1), 4–28.
- (46) Estey, T.; Kang, J.; Schwendeman, S. P.; Carpenter, J. F. *J. Pharm. Sci.* **2006**, *95* (7), 1626–39.
- (47) Togashi, D.; Ryder, A.; O'Shaughnessy, D. *J. Fluoresc.* **2010**, *20* (2), 441–452.
- (48) Hawkins, M. J.; Soon-Shiong, P.; Desai, N. *Adv. Drug Delivery Rev.* **2008**, *60* (8), 876–885.
- (49) Iancu, C.; Mocan, L.; Bele, C.; Orza, A. I.; Tabaran, F. A.; Catoi, C.; Stiufluc, R.; Stir, A.; Matea, C.; Iancu, D.; Agoston-Coldea, L.; Zaharie, F.; Mocan, T. *Int. J. Nanomed.* **2011**, *6*, 129–41.
- (50) Patel, N. R.; Pattni, B. S.; Abouzeid, A. H.; Torchilin, V. P. *Adv. Drug Delivery Rev.* **2013**, *65* (13–14), 1748–1762.